Appl Phys B (2009) 97: 887–895
DOI 10.1007/s00340-009-3620-y

Applied Physics B
Lasers and Optics

Simultaneous flow field and fuel concentration imaging at 4.8 kHz in an operating engine

B. Peterson · V. Sick

Received: 17 March 2009 / Revised version: 28 May 2009 / Published online: 30 June 2009

Abstract High-speed particle image velocimetry (PIV) and planar laser induced fluorescence (PLIF) techniques are combined to acquire flow field and fuel concentration in a spray-guided spark-ignited direct-injection (SG-SIDI) engine under motored and fired operation. This is a crucial step to enable studies that seek correlations between marginal engine operation (misfires or partial burns) and local, instantaneous mixture and flow conditions. Correlated flow and fuel data are extracted from a 4 mm × 4 mm sub-region directly downstream the spark plug to characterize the in-cylinder conditions next to the spark plug during the spray and ignition event. Values of equivalence ratio, velocity magnitude, shear strain rate, and vorticity all increase during the spray event and decrease an order of magnitude during the duration of the spark event.

PACS 42.62.Fi · 47.80.-v · 06.60.Jn

1 Introduction

Spray-guided spark-ignition direct-injection (SG-SIDI) engines offer the potential to improve fuel economy and emissions for gasoline internal combustion (IC) engines [1]. The spray-guided concept relies heavily on the interaction between the spray event and spark event for ignition. Fuel spray is delivered directly to the vicinity of the spark plug with spark timing optimized to provide reliable ignition. During low- to mid-loads, fuel is injected late within the compression stroke producing a highly stratified mixture within the combustion chamber, particularly next to the spark plug. The spark event typically occurs during the spray event or within a few crank-angle degrees (CAD) afterwards when an ignitable mixture is within the vicinity of the spark plasma.

The very method used to deliver an ignitable air–fuel mixture to the spark plug can produce high velocity magnitudes, large velocity gradients, and large fuel concentration gradients—all which have the potential to adversely affect the spark and ignition process. High velocity magnitudes nearby the spark plug can extinguish the spark plasma leading to multiple restrikes and shorter spark durations [2, 3]. Fansler et al. [4] identify local flow velocity fluctuations as the cause of unfavorable spark motion and location which lead to rare and random ignition failures (misfires). Flame extinction from high strain rates has been shown, e.g., for laminar diffusion flames [5, 6] and turbulent counterflow premixed flames [7]. Large values of strain rate can indicate high scalar dissipation rates which can ultimately increase heat loss from the flame and can cause flame extinction [8]. Fluid rotation (vorticity) is another parameter of interest which has the ability to distort the flame front [8–10].

Highly stratified mixtures expose the spark plasma to a wide variety of air–fuel concentrations within a short time period. If the spark plasma does not come in contact with a favorable mixture for ignition, misfires or partial burns are likely to occur [1, 2, 11].

Hence, it is important to study both flow field characteristics and fuel distribution near the ignition site to gain a better understanding of the in-cylinder conditions that influence the ignition quality in a SG-SIDI engine. It will be important to measure flow and fuel distribution simultaneously and in multiple dimensions, i.e., imaging diagnostics

B. Peterson (✉) · V. Sick
Department of Mechanical Engineering, The University of Michigan, 2026 W. E. Lay Automotive Laboratory, 1231 Beal Ave., Ann Arbor, MI 48109-2133, USA
e-mail: bpete@umich.edu
Fax: +1-734-7644256

must be used. Furthermore, since the spark event typically lasts only a few milliseconds, it is critical that the temporal evolution is observed within individual engine cycles to capture the variation of flow and mixture conditions. Crank angle resolution (here 208 µs image separation) should be adequate for such studies [4, 12–14]. Combined high-speed imaging techniques for flow and fuel measurements in engines have been demonstrated but have not been applied simultaneously in engines [15].

This work describes the simultaneous application of particle image velocimetry (PIV) and planar laser induced fluorescence (PLIF) of biacetyl at a rate of 4.8 kHz to simultaneously capture flow field and fuel concentration images at crank-angle resolution during the spray and spark events in a SG-SIDI engine under motored and fired operation. This study is designed to show that the two high-speed measuring techniques can be used simultaneously in an operating engine under motored and fired operation. Engine operating parameters used in this study provide stable engine operation (no misfires or partial burns). Once it is demonstrated that reliable measurements can be obtained, future studies can address marginal engine operation to identify the physical and chemical causes of misfires and partial burns.

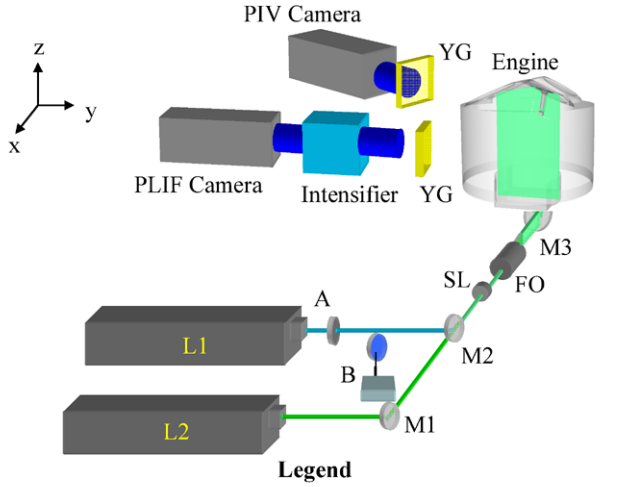

Fig. 1 Green laser light at 527 nm and UV laser light at 355 nm were used for the combined PIV and PLIF experiments. The PLIF camera and intensifier were perpendicular to the imaging plane inside the engine, while the PIV camera was at a 15° angle with a lower aperture setting

2 Experimental

2.1 Optical setup

A frequency-doubled Nd:YLF 527 nm (Quantronix Darwin Duo) dual cavity laser was used as the light source for Mie scattering images for PIV measurements. Each laser beam was circularly polarized and had a diameter of ∼15 mm. At 4.8 kHz, each laser beam provided 5.9 mJ of energy per pulse. A frequency-tripled Nd:YAG 355 nm (Quantronix Hawk I) laser was used for the fluorescence measurements. The UV laser beam was linearly polarized and had a diameter of ∼5 mm. At 4.8 kHz the laser provided 1.4 mJ of energy per pulse.

The optical setup used to deliver the laser light into the combustion chamber was optimized so that the UV and green laser sheets were of comparable thicknesses and focused on the same region of interest. A high-reflectivity (HR) 355 nm, high-transmissivity (HT) 532 nm turning mirror was used to reflect UV laser light towards the engine, while allowing the green laser light to pass through. This combined the UV and green laser beams in the same optical path towards the engine. A spherical lens was used to focus the laser beams into a telescope with a set of cylindrical lenses (LaVision) to diverge the laser beam into a sheet. The laser sheets entered a hole in the engine crankcase and were reflected off a 45° UV coated mirror, providing a vertical plane for the light sheets inside the combustion chamber as shown in Fig. 1. The vertical light sheets were aligned with the tumble plane and bisected the fuel injector and spark plug. The higher intensity region of each laser sheet was aligned directly downstream of the spark plug to provide as much light as possible for Mie scattering and fluorescence at this location. Optical components were tuned to produce similar light sheet thicknesses (1 mm) for both the green and UV laser sheets at the location of the spark plug ground strap. The UV laser sheet had a slightly smaller width (∼20 mm) than the green laser sheets (∼35 mm) due to the smaller beam diameter.

A 12-bit CMOS camera (Vision Research Phantom V7.1) was used to capture the Mie scattering of green light off of silicone oil droplets (∼1 µm diameter) which were seeded into the intake air [13], while a 14-bit CMOS camera (Vision Research Phantom V7.3) equipped with a lens-coupled image intensifier (LaVision HS-IRO) was used to capture the fluorescence of the biacetyl component of the fuel mixture. The fluorescence signal was focused onto the intensifier with a Nikkon 105 mm (f#1.2) lens. Without such devices as a beam splitter, it was not possible to orient both cameras perpendicular to the light sheets in the tumble plane. Since the energy of the green laser light was greater than the UV laser light, it was plausible to orient the PIV camera at a slight angle (∼15° off the normal to the light sheet) to the tumble plane and decrease the aperture of the camera to increase the depth of field. The PLIF camera and intensifier were set up

perpendicular to the light sheet in the tumble plane. Yellow glass filters were placed in front of each camera to mitigate Mie scattering of droplets below 400 nm.

A photodiode (LaVision) was used to capture UV light reflected off the spherical lens to provide a measure of the UV laser energy during the course of the experiment and from experiment to experiment.

2.2 Engine

The optical SG-SIDI engine is shown in full in Fig. 2(a). The main components of the engine consist of a General Motors prototype, twin-cam, overhead-valve, pentroof aluminum cylinder head, a full quartz-glass cylinder, and a quartz-glass Bowditch piston. The quartz-glass cylinder granted optical access from the side as demonstrated in Fig. 1. Quartz-glass windows installed within the cylinder head granted optical access of the spark-plug region and fire deck. In addition, side windows within the piston bowl (Fig. 2(b)) provided optical access within the piston bowl as the piston moved up toward top-dead-center (TDC). The quartz-bottom piston allowed the vertical laser light sheets to enter into the combustion chamber.

Fig. 2 (**a**) Optical engine with quartz glass cylinder, (**b**) Bowditch piston with quartz bottom and side windows, (**c**) view of cylinder head showing spray plume direction (*arrows*) with respect to spark plug orientation and location of laser light sheet (bisecting the fuel injector and spark plug)

A 90° multi-hole (8 hole) injector and a double-pinned spark plug were used in the engine. One of the holes of the injector was aimed at the spark plug to provide a spray plume that impacted the spark plug as shown in Fig. 2(c). The spark plug was oriented with the ground strap perpendicular to the tumble plane and pointed in the direction of the high-speed cameras.

2.3 Operating parameters

Engine operating conditions, shown in Table 1, were chosen to mimic low-load operating conditions in a SG-SIDI engine. For the cases of motored-spray, the spark event was not executed. Air jets were used to cool the quartz cylinder during the course of the experiment. Due to safety issues of overheating, the engine did not run in fired operation longer than 5 minutes. Operating parameters shown provided stable engine operation (no misfires or partial burns) with a coefficient of variation (COV) of indicated mean effective pressure (IMEP) $< 4\%$.

The fuel used for this study was a mixture of 90% isooctane, 10% biacetyl (percentage by volume). This mixture was chosen to provide known fluorescence characteristics (excited biacetyl at 355 nm and red-shifted fluorescence [14, 16]), while not diverging from typical combustion characteristics seen from the fuel blend typically used in the automobile engine.

Optical parameters of the imaging equipment are also shown in Table 1. Note that the depth of focus for the PIV camera is much greater than the PLIF camera (order of magnitude) allowing the Mie scattering to be captured with the PIV camera at a slight angle to the tumble plane.

Trigger signals indicating each CAD and cycle were sent to a high-speed controller (LaVision), which was used in conjunction with the imaging system (LaVision-DaVis) to control the timing of the cameras and lasers and their synchronization with the engine. A Hall-effect sensor was used

Table 1 Operating parameters for experiments in the optical SG-SIDI engine

Engine parameters		Optical parameters	
Engine speed	800 RPM	PLIF intensifier exposure time	300 ns
Intake manifold pressure	95 kPa (absolute)		
Intake air temp.	45°C	Intensifier gain	6.0
Coolant temp.	45°C	PLIF camera aperture	2.8
Injection timing	36–32° BTDC	PLIF camera depth of focus	0.3 mm
Injection pressure	110 bar	PLIF camera exposure time	150 µs
Fuel	90% isooctane, 10% biacetyl	PIV camera aperture	11.0
Fuel per cycle	∼7.5 mg	PIV camera depth of focus	2.3 mm
Spark timing	32–24° BTDC		

with the engine flywheel to indicate each CAD of the piston, while another Hall-effect sensor was used with the cam flywheel to indicate the occurrence of a new engine cycle. Each laser fired once during every CAD giving three laser pulses per CAD. Three images were taken each CAD from 46° BTDC to 4° ATDC, giving two Mie scattering images for PIV measurements and one fluorescence image for PLIF measurements. The PIV camera split each crank-angle into two temporally equal frames of 104 µs in which the camera took one image in each frame. The two green laser pulses were separated by a time delay of 15 µs to capture as much of the spray velocity as possible and provided a pixel shift that was within 1/4 of the final interrogation window size (32 × 32) [17]. The UV laser fired 24 µs after the second green laser pulse; the intensifier was open for 300 ns and the PLIF camera captured the fluorescence image with an exposure time of 150 µs.

2.4 Experimental procedure

A set of three engine runs were conducted for a given experiment to obtain Mie scattering and fluorescence images and further process these images into vector fields and fuel concentration measurements. After each run, the engine was spun down and the images were saved. The first run consisted of 150 consecutive cycles for the experiment of interest—PIV and PLIF measurements under late injection and stratified charge. Here seeding was introduced into the intake air for PIV measurements and fuel was injected late within the compression stroke (36–32° BTDC). The second run consisted of what will be denoted as lightsheet images. Here a known amount of fuel was injected early within the intake stroke (250° BTDC) to produce a quasi-homogeneous fuel-air mixture within the combustion chamber. This run consisted of 100 cycles used for averaged cycle analysis and was used solely for the PLIF processing routine to normalize the fuel concentration within the late injection run. Seeding was not used for this run. Finally, the third run consisted of 100 cycles of background images for both the PIV and PLIF images without fuel injection or PIV seeding. Only the lasers were fired to provide a background image used to subtract background noise. This procedure was used for both motored and fired experiments, with each experiment conducted separately.

2.5 Data processing

A commercial imaging software program (LaVision DaVis 7.1) was used for processing the PIV and PLIF images. The two Mie scattering images were cross correlated with decreasing size multi-pass iterations. An initial window size of 128 × 128 was reduced to a final window size of 32 × 32 with 50% overlap and two passes for each reduction in window size. The 32 × 32 interrogation window corresponded to a 2.8 mm × 2.8 mm region with vectors shown every 1.4 mm with the 50% overlap. During vector post-processing, the peak ratio factor, Q, was set to 1.8 to improve the accuracy of the vector computation. Spurious vectors present in the original vector field were eliminated by using a median filter which removed vectors which had x and y vector components that differed greater than $U_{\text{median}} \pm 2U_{\text{rms}}$ of its neighboring vectors. The vectors were re-inserted with the average weight of its neighboring vectors if the vector was within $U_{\text{median}} \pm 3U_{\text{rms}}$ of its neighboring vectors. This procedure removed spurious vectors while preserving vector gradient information. A 3 × 3 Gaussian smoothing filter was applied to the vector field to remove noise at spatial scales near the resolution limit of the PIV measurements [18].

The averaged background and lightsheet images for PLIF were normalized with respect the UV laser energy measurement from the photodiode. The late injection fluorescence images and lightsheet images were corrected by subtracting the averaged background images. The late injection images were then normalized by the lightsheet images to provide a scaled signal representative of equivalence ratio. It has been demonstrated that normalization of the late injection images by images of known and homogeneous fuel concentration provides a LIF signal that becomes a representation of the equivalence ratio [12, 14, 19]. Normalizing of these images also accounts for pressure and temperature dependencies of the LIF signal from the biacetyl and laser light sheet inhomogeneities [12]. A non-linear sliding average filter of size 5 pixels was applied to the late injection fuel distribution image to smooth the fuel concentration within the region of 5 × 5 pixels (0.35 mm × 0.35 mm). A mask was used to remove saturated signals in such region as the cylinder head. The vector field was then overlaid onto the processed PLIF images and an overlay was used to clarify the position of significant features such as the spark plug and injector.

3 Results

3.1 Simultaneous flow field and fuel concentration images

Simultaneous flow field and fuel concentration measurements were obtained at crank-angle resolution in a SGSIDI single-cylinder optical engine under stratified operation for motored-spray and fired cycles. Measurements were made along the tumble plane bisecting the injector and spark plug. Fuel concentration measurements were confined to a 17 mm × 28 mm region near the spark plug, while velocity measurements expanded a slightly larger region of 28 mm × 28 mm as illustrated in Fig. 3. The different dimensions of the two measurement planes are due to the differences in light sheet width between the UV and green lasers. As previously mentioned, the UV laser sheet spanned a horizontal distance of ∼20 mm, while the green laser sheets

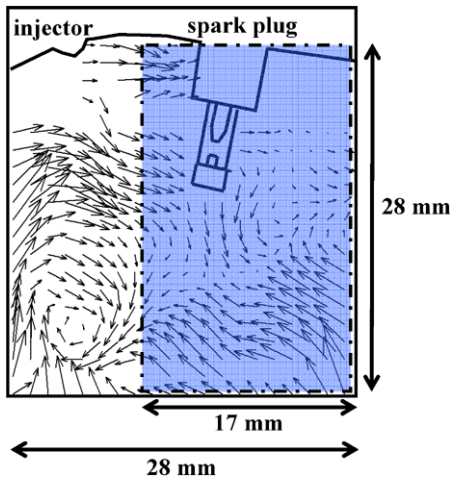

Fig. 3 Fuel concentration measurements were confined to a 17 mm × 28 mm region (*darkened region*), while velocity measurements were obtained in a 28 mm × 28 mm viewing plane

spanned a distance of ∼35 mm. For both UV and green lasers, the portion of highest laser intensity was concentrated in the region directly downstream of the spark plug.

Analysis of these measurements is intended to understand the in-cylinder conditions that exist near the spark plug during ignition. Measurements were performed for motored and fired operation. Measurements made under motored operation provide baseline measurements without the interference of combustion luminosity.

Images of flow field and fuel concentration during the spray event under motored operation are shown for a single cycle in Fig. 4(a)–(l). The spray event (36–32° BTDC) is adequately depicted in Fig. 4(a)–(e), while post-spray images are shown in the succeeding images of Fig. 4. A clockwise tumble motion is disrupted by the spray event, but is then retained to some degree a few degrees after the end-of-spray.

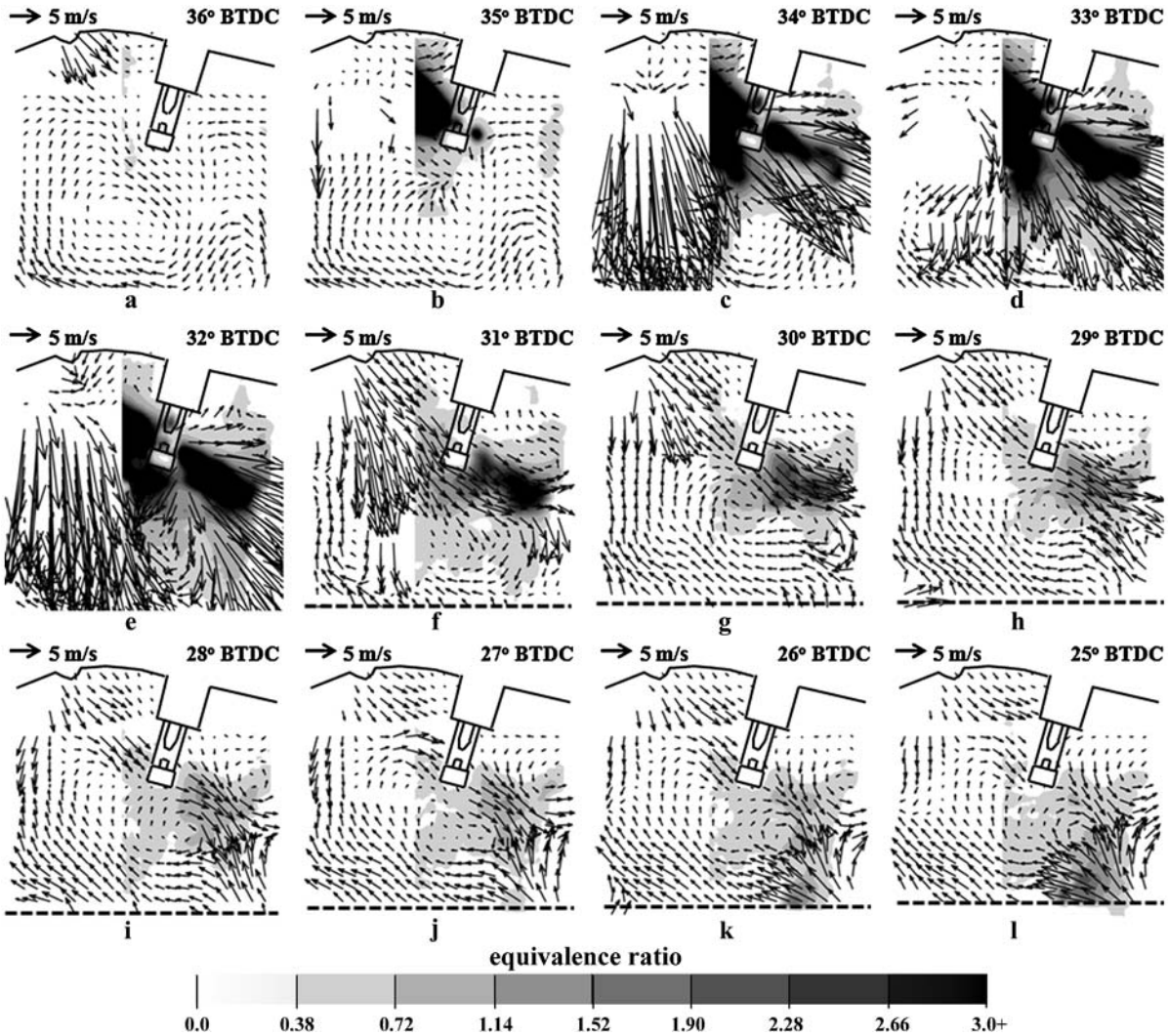

Fig. 4 Simultaneous fuel concentration and velocity measurements illustrate the strong coupling of spray momentum and air–fuel mixing inside a SG-SIDI engine

It is shown that the spray plume impacts the spark plug where a portion of the fuel passes through the spark gap, while another portion of the fuel impacts the ground strap and is reflected downward. The momentum of the air–fuel mixture continues diagonally downward into the piston bowl and impacts the bottom corner of the piston bowl. The fluid then rebounds off the piston bowl surface causing the flow to reverse direction near the bottom right corner (Fig. 4(g)–(l)). The bottom corner of the piston bowl is not shown within the viewing plane, but the bottom of the piston bowl is indicated by the dashed line (Fig. 4(f)–(l)).

Velocity details of the spray event are adequately captured in most of the images shown. Areas of intense Mie scattering that saturate the camera lead to a calculation of erroneous vectors and were therefore not considered in the velocity calculation. This explains the "gaps" within the velocity field on the left-hand side of Fig. 4(b) and (d) and the reason why velocity is not shown within the fuel plume passing through the spark plug. Velocities near the edges of the spray plume are resolved and representative of the spray velocities.

Details of the fuel distribution demonstrate that a rich fuel plume is present downstream of the spark plug shortly after the end-of-spray (31° BTDC). Succeeding this image, the fuel plume is dispersed into a less compact fuel cloud which moves downward and to the right of the image where fuel vapor is then collected within the piston bowl and moves upward with the bottom of the piston bowl (Fig. 4(k)–(l)). Velocities surrounding the fuel cloud further elaborate the motion of the air–fuel mixture downstream of the spark plug and within the piston bowl.

Previous PIV studies in this SG-SIDI engine with late injection have shown that the flow prior to the injection event is primarily 2-dimensional and becomes highly 3-dimensional during the spray event [13]. Even though the flow field is 3-dimensional during the spray event, the 2-dimensional details shown in Fig. 4 adequately describe the spray and evolution of the resulting air–fuel mixture.

3.2 In-cylinder measurements near the spark plug under motored and fired operation

The ultimate goal of the simultaneous measurements is to understand in-cylinder mixing and flow conditions seen by the spark plasma and their relation to successful ignition under highly stratified conditions. Therefore, further analysis of the measurements was focused in a 4 mm × 4 mm region directly downstream of the spark plug as illustrated in Fig. 5.

Spatial averages of normalized fuel concentration (equivalence ratio ($\overline{\phi}$)), velocity magnitude ($|\overline{V}|$), shear strain rate magnitude ($|\overline{\frac{1}{2}(\frac{\partial u}{\partial y}+\frac{\partial v}{\partial x})}|$), and vorticity magnitude ($|\overline{\frac{\partial u}{\partial y}-\frac{\partial v}{\partial x}}|$) were extracted from the 4 mm × 4 mm region next to the spark plug. Quantities represented as ($\overline{\ }$) denote

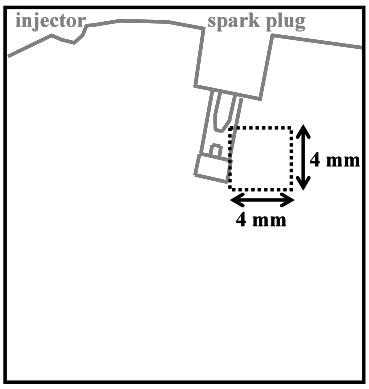

Fig. 5 Velocity quantities and fuel concentrations were extracted from a 4 mm × 4 mm sub-region directly downstream of the spark plug in order to understand in-cylinder conditions as seen by the spark plasma

the spatial average. Measurements were obtained for motored and fired cycles from 46° BTDC to 4° ATDC. Motored operation and fired operation were conducted as separate experiments, each consisting of 150 consecutive engine cycles. The engine was fired continuously under fired operation.

For fired cycles, measurements past 25° BTDC were ignored due to interference from combustion luminosity. Combustion luminosity increased the signal recorded by the PLIF camera resulting in an erroneous fuel concentration measurement. In addition, flame luminosity produced correlations between the PIV camera frames giving velocities related to flame propagation.

Strain rate (fluid deformation) and vorticity (fluid rotation) are parameters of interest because their contribution to wrinkle and distort a flame kernel. As previously mentioned, high strain rates have the ability to extinguish a flame kernel.

3.2.1 Fuel concentration

Crank-angle resolved measurements of the spatial average equivalence ratio ($\overline{\phi}$) distinctly depict fuel concentrations near the spark plug during the spray event and post-spray event for both motored and fired cycles. Values shown in Fig. 6 are ensemble averages over 150 cycles, with error bars indicating one standard deviation from the 150 measurements at each given crank angle. Fuel concentrations begin to increase at 35° BTDC when the fuel plume first arrives at the spark plug as demonstrated in Fig. 4(b). Equivalence ratio increases substantially (from $\langle\overline{\phi}\rangle = 0.6$ to $\langle\overline{\phi}\rangle \geq 6.0$, where $\langle\,\rangle$ indicates the ensemble average) one crank-angle degree later (34° BTDC) when a fuel plume is within the 4 mm × 4 mm region. A wide range of rich air–fuel mixtures are measured throughout the spray event (36–32° BTDC) and shortly afterwards (31° BTDC) as indicated by the error bars. Mixtures lean out quickly after the spray event ($\langle\overline{\phi}\rangle = 2.7$ at 31° BTDC to $\langle\overline{\phi}\rangle = 1.1$ at 29° BTDC) and become predominately lean after 27° BTDC where $\langle\overline{\phi}\rangle < 0.8$ for the remainder of the compression stroke.

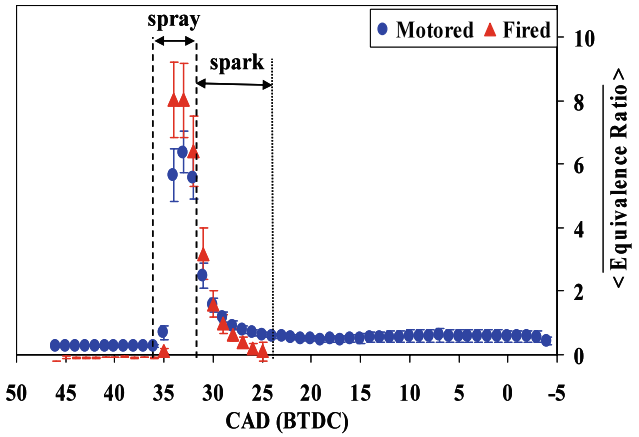

Fig. 6 The error bars indicate a one-standard deviation range of the equivalence ratio and show that equivalence ratio varies significantly from cycle-to-cycle during the spray event and leans out quickly afterwards ($\langle\overline{\phi}\rangle = 2.7$ at 31° BTDC to $\langle\overline{\phi}\rangle = 1.1$ at 29° BTDC). Ensemble averages of the spatial average of equivalence ratio remain fuel-lean $\langle\overline{\phi}\rangle < 0.8$ after 27° BTDC

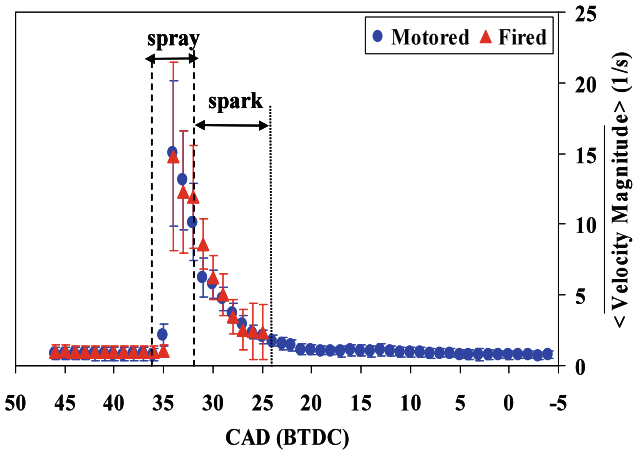

Fig. 7 Velocity magnitude and its standard deviation (indicating cycle-to-cycle variation) downstream the spark plug both increase an order of magnitude during the spray event. A wide range of velocity magnitudes exist during spark timing; $\langle\overline{V}\rangle = 11$ m/s at the onset of spark (32° BTDC) and continually decrease to $\langle\overline{V}\rangle = 1.5$ m/s by 24° BTDC at the end of spark

It is shown that values of equivalence ratio before the spray event are positive under motored operation while zero under fired operation. Under fired operation, the fuel mixture is almost entirely consumed during combustion leaving combustion products within the cylinder. A portion of these combustion products remain in the cylinder during the exhaust and intake stroke as residual gas and are present during the next cycle. This residual gas does not contain the fluorescing fuel mixture and therefore does not result in a fluorescence signal until fuel is injected within the cylinder. Under motored operation, combustion does not take place and the residual gas consists of the fluorescing fuel mixture giving a positive value of fuel concentration before the spray event.

In some instances, the measured fuel concentration under fired operation is negative with values as low as −0.1. This is the case before fuel is injected; note that in contrast to motored engine operation, there is no residual fuel present from previous cycles. The engine was cleaned after the completion of the three runs of each measurement set (1. late injection, 2. lasersheet, 3. background). At this time, silicone oil droplets were present on the piston and cylinder. The droplets were yellow in color indicating that biacetyl was dissolved in these otherwise transparent droplets. This suggests the presence of some biacetyl in the combustion chamber during the background run that might produce a measurable LIF signal. Subtracting the background images from the late injection images will then result in an apparent negative equivalence ratio. It is also possible that deposits build up on the quartz windows and cylinder liner so that transmission changes over time to affect laser or LIF signal transmission. Alternating imaging between the three runs within a single experiment should be programmed with the engine set point controller to minimize the impact of drifts in the background image scaling.

During the spray event, liquid fuel is present in the 4 mm × 4 mm region near the spark plug. Fluorescence signal strength of liquid biacetyl has not yet been characterized for engine conditions. The normalization of late injection images in the presence of liquid might therefore not completely render the results quantitative as is the case for fully vaporized conditions. Mie scattering images from the PIV measurements show that all but a few droplets are vaporized at the end-of-spray (30° BTDC). This indicates that the fluorescence signal beyond this crank angle is solely due to the fluorescence of the biacetyl vapor.

3.2.2 *Velocity magnitude*

Figure 7 shows crank-angle resolved measurements of velocity magnitude ($\overline{V}$) near the spark plug during the spray and post-spray events. Values are ensemble averages ($\langle\rangle$) over 150 cycles, with error bars indicating one standard deviation from the 150 measurements at each given crank angle. Velocity magnitude increases dramatically during the spray event (from $\langle\overline{V}\rangle = 1.0$ m/s at 36° BTDC to $\langle\overline{V}\rangle =$ 15 m/s at 34° BTDC). Cycle-to-cycle variations of velocity magnitude are also shown to increase during the spray event as indicated by the order of magnitude increase in standard deviation (±0.5 m/s before 36° BTDC to ±5.0 m/s from 34–32° BTDC). Velocities seen at the beginning of ignition timing are relatively high ($\langle\overline{V}\rangle = 11$ m/s at 32° BTDC) and decrease an order of magnitude throughout the remainder of spark timing ($\langle\overline{V}\rangle = 1.5$ m/s at 24° BTDC). Well after the spray event (20° BTDC) velocity magnitude decreases to similar values measured before the spray event

($\langle\overline{V}\rangle < 1$ m/s). Velocity measurements for motored and fired cycles are shown to agree in magnitude.

3.2.3 *Shear strain rate and vorticity*

Figure 8 shows the ensemble average of the magnitude of the spatial average for shear strain rate

$$\left\langle\left|\overline{\frac{1}{2}\left(\frac{\partial u}{\partial y}+\frac{\partial v}{\partial x}\right)}\right|\right\rangle \quad \text{and vorticity} \quad \left\langle\left|\overline{\frac{\partial u}{\partial y}-\frac{\partial v}{\partial x}}\right|\right\rangle$$

that were obtained from the motored and fired flow fields. Velocity gradients measured before the spray event are shown to be relatively low ($\sim 125 \pm 50$ s^{-1} for shear strain rate and $\sim 250 \pm 100$ s^{-1} for vorticity). The spray event dramatically increases shear strain rate (1700 s^{-1}) and vorticity (1900 s^{-1}) at 34° BTDC with large cycle-to-cycle variations as indicated by the error bars ($\pm$600–1000 s^{-1}). Both shear strain rate and vorticity are shown to ultimately decrease during the spark timing. Shear strain rate (fluid deformation) continually decreases through the remaining part of compression to values measured before the spray event, while the vorticity (fluid rotation) sharply decreases at the end of the spark event and remains relatively constant ($\sim$400 s^{-1}) throughout the remainder of the compression stroke.

Larger cycle-to-cycle variability exists for fired cycles near the end of the spark event because a flame kernel often develops in this region causing the fluid to disperse quickly creating a wide variety of velocity gradients.

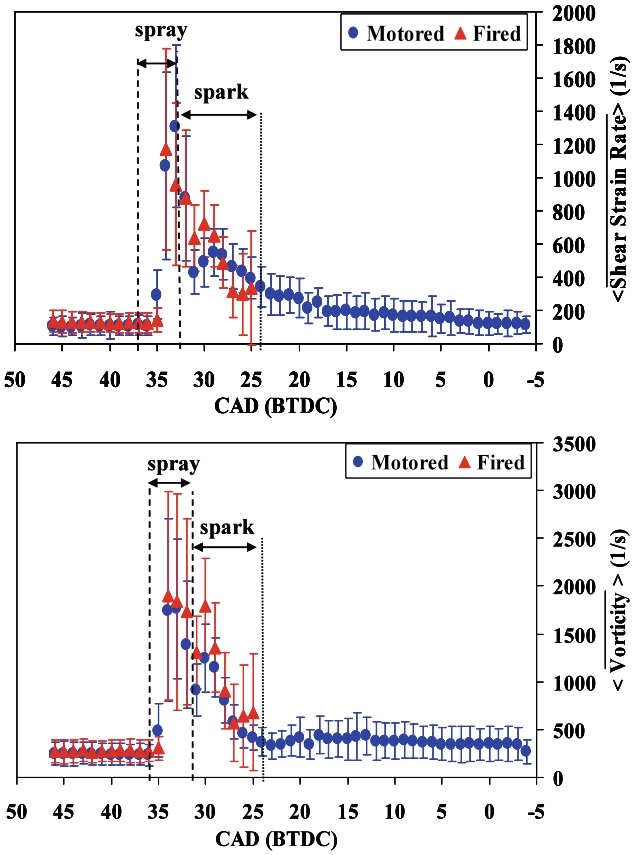

Fig. 8 Shear strain rate and vorticity near the spark plug increase by an order of magnitude from spray. Shear strain rate decreases throughout spark timing and throughout the remainder of the compression stroke, while vorticity decreases throughout spark timing and then remains relatively constant throughout the remainder of the compression stroke

3.2.4 *Correlation of fuel concentration and velocity magnitude*

The spatial averages of equivalence ratio and velocity magnitude within the 4 mm × 4 mm region are plotted against one-another to understand the relationship between fuel concentration and flow field during and after the spray event. Figure 9 shows the spatially averaged measurements during spray (36–32° BTDC), directly after spray (31° BTDC), and after spray (30° to −4° BTDC) for 150 motored cycles. Measurements at 36° and 35° BTDC (during the early part of the spray event) result in low velocity and equivalence ratio values because the fuel plume is not present within the 4 mm × 4 mm region downstream the spark plug. These measurements are not shown in Fig. 9 in order to highlight the critical measurements during the spray event (34–32° BTDC) and to clearly show the measurements of lower velocity and equivalence ratio well after the spray event (30° to −4° BTDC).

During spray, velocity magnitude is shown to cover a wide range of values ($\overline{V} = 4.4$–29 m/s) over the 150 cycles. Equivalence ratio is shown to span a slightly smaller range of values ($\overline{\phi} = 3.8$–8.0). This clearly demonstrates the large cycle-to-cycle variation and stochastic behavior of the in-cylinder flow and mixture during the spray event. Directly after the spray event (31° BTDC), a rich fuel plume ($\overline{\phi} = 1.6$–3.6) is often present downstream of the spark plug as indicated in Fig. 4d. Velocity values at this time are reduced ($\overline{V} = 3.5$–9.5 m/s) as the momentum behind the fuel plume has decreased. After the spray event (30° to −4° BTDC), velocity and equivalence ratio values show a decaying trend throughout the remainder of the compression stroke. This decaying trend can also be demonstrated in Figs. 6 and 7, where equivalence ratio measurements decrease from 30–25° BTDC and remain relatively constant throughout the remainder of the compression stroke, while velocity measurements continue to decay after the spray event.

4 Conclusions

High-speed particle image velocimetry and planar laser induced fluorescence of biacetyl were combined and applied

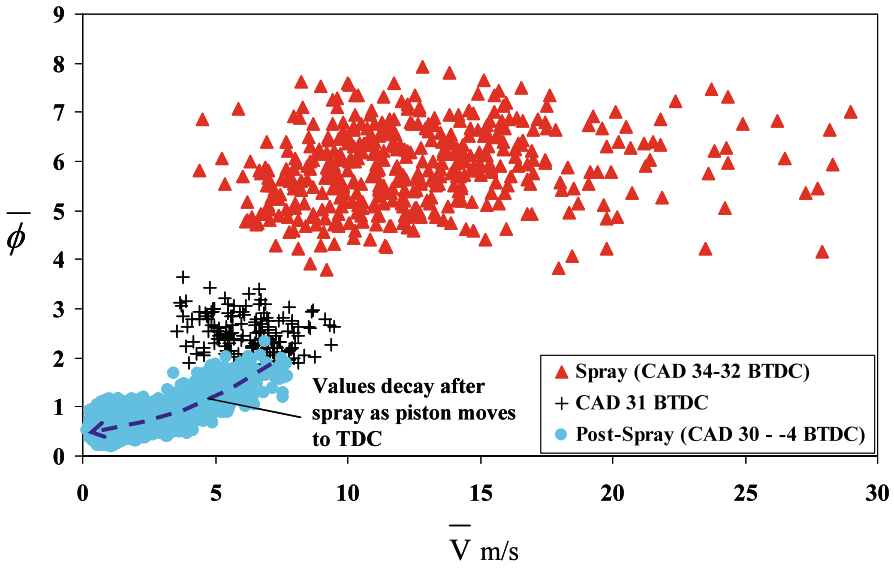

Fig. 9 Spatial averages of fuel concentration and velocity magnitude from 150 motored cycles distinctly show the range of values that exist during the spray event, after the spray event, and during the rest of compression

in a SG-SIDI optical engine to obtain simultaneous measurements of flow field and fuel concentration under late-injection for motored and fired cycles. Velocity gradient information was extracted from the flow field to provide additional information about fluid deformation (shear strain rate) and fluid rotation (vorticity) in the vicinity of the spark plug.

Measurements focused on a region near the spark plug and demonstrate the capability to capture pertinent in-cylinder conditions that exist prior and during the ignition event. The measurements show a substantial increase in equivalence ratio, velocity magnitude, shear strain rate, and vorticity values with large cycle-to-cycle variations during the spray event. A large range of values are also shown to exist during the spark event as large cycle-to-cycle variations still exist as well as a continual decrease in values after the end of spray.

This diagnostic technique is shown to provide measurements for both motored and fired cycles. Engine parameters were optimized to obtain stable engine operation for combustion cases (low coefficient of variance (COV) and high indicated mean effective pressure (IMEP)). Future work will consist of obtaining simultaneous flow field and fuel concentration measurements for conditions of unstable engine operation (misfire and partial burns) to understand the in-cylinder conditions that influence the ignition event leading to successful and unsuccessful combustion. It will be necessary to study crank-angle resolved measurements pertaining to individual cycles to understand the impact of these conditions on ignition events.

Acknowledgements This work was supported through the General Motors Collaborative Research Laboratory on Engine Systems Research at the University of Michigan. The authors are grateful for contributions to the experiment from M. Mosburger, M. Cundy, and A. Alharbi.

References

1. F. Zhao, M.-C. Lai, D.L. Harrington, Progr. Energy Combust. Sci. **25**, 437–562 (1999)
2. R. Maly, in *Fuel Economy in Road Vehicles powered by Spark Ignition Engines*, ed. by J.C. Hilliard, G.S. Springery (Plenum Press, New York, 1984), p. 453
3. J.D. Smith, V. Sick, SAE Paper 2006-01-3376 (2006)
4. T. Fansler, M. Drake, B. Böhm, in *8th International Symposium on Internal Combustion Diagnostics*, Baden-Baden (2008)
5. H. Tsuji, I. Yamaoka, Proc. Combust. Inst. **11**, 1979 (1967)
6. R.G. Abdel-Gayed, D. Bradley, M.N. Hamid, M. Lawes, Proc. Combust. Inst. **20**, 505–512 (1984)
7. D. Bradley, Proc. Combust. Inst. **24**, 247–262 (1992)
8. J. Warnatz, U. Maas, R.W. Dibble, *Combustion*, 2nd edn. (Springer, Berlin, 1999)
9. D.A. Eichenberger, W.L. Roberts, Combust. Flame **118**, 469–478 (1999)
10. A.M. Steinberg, J.D. Driscoll, S.L. Ceccio, Proc. Combust. Inst. **32**, 1713–1721 (2009)
11. J.D. Smith, PhD thesis, The University of Michigan, Ann Arbor, 2006
12. J.D. Smith, V. Sick, Appl. Phys. B **81**, 579–584 (2005)
13. C.M. Fajardo, V. Sick, Proc. Combust. Inst. **31**, 3023–3031 (2007)
14. J.D. Smith, V. Sick, Proc. Combust. Inst. **31**, 747–755 (2007)
15. C.M. Fajardo, J.D. Smith, V. Sick, Appl. Phys. B **85**, 25–30 (2006)
16. N. Wermuth, V. Sick, SAE Trans. J. Fuels Lubr. **114**, 804–814 (2005)
17. R. Adrian, Meas. Sci. Technol. **8**, 1393–1398 (1997)
18. C.M. Fajardo, V. Sick, D.L. Reuss, *PIV 2007* (2007)
19. S. Einecke, C. Schulz, V. Sick, Appl. Phys. B **71**, 717–723 (2000)